INTERNATIONAL JOURNAL FOR NUMERICAL METHODS IN FLUIDS
Int. J. Numer. Meth. Fluids 2003; **41**:495–518 (DOI: 10.1002/fld.444)

A fourth-order compact finite difference scheme for the steady stream function–vorticity formulation of the Navier–Stokes/Boussinesq equations

Zhenfu Tian[1,2,*,†] and Yongbin Ge[3]

[1]*Institute of Applied Mathematics & Engineering Mechanics, Ningxia University, Yinchuan, Ningxia 750021, China*
[2]*Shanghai Institute of Applied Mathematics & Mechanics, Shanghai University, Shanghai 200072, China*
[3]*School of Power Engineering, University of Shanghai for Science and Technology, Shanghai 200093, China*

SUMMARY

A fourth-order compact finite difference scheme on the nine-point 2D stencil is formulated for solving the steady-state Navier–Stokes/Boussinesq equations for two-dimensional, incompressible fluid flow and heat transfer using the stream function–vorticity formulation. The main feature of the new fourth-order compact scheme is that it allows point-successive overrelaxation (SOR) or point-successive underrelaxation iteration for all Rayleigh numbers *Ra* of physical interest and all Prandtl numbers *Pr* attempted. Numerical solutions are obtained for the model problem of natural convection in a square cavity with benchmark solutions and compared with some of the accurate results available in the literature.

KEY WORDS: Navier–Stokes/Boussinesq equations; stream-function-vorticity formulation; compact scheme; natural convection; heated cavity problem

1. INTRODUCTION

This paper is primarily aimed at developing a fourth-order compact finite difference (FD) scheme to solve the steady-state stream function–vorticity form of the two-dimensional, incompressible Navier–Stokes/Boussinesq equations governing the fluid flow and heat transfer.

* Correspondence to: Z. Tian, Institute of Applied Mathematics & Engineering Mechanics, Ningxia University, Yinchuan, Ningxia 750021, China.
† E-mail: zftian@nxu.edu.cn

Contract/grant sponsor: National Natural Science Foundation of China; contract/grant number: 19702008
Contract/grant sponsor: High Performance Computing Foundation of China; contract/grant number; 99107 and 00108

Received June 2001
Revised 10 August 2002

It is known that FD methods of obtaining approximate numerical solutions of the steady-state incompressible Navier–Stokes/Boussinesq equations can vary considerably in terms of accuracy and efficiency. In the area of finite differences, the most familiar schemes are the central differences and the so-called upwind differences [1]. It has been discovered that although central difference approximations have a truncation error of order h^2, they often suffer from computational instability and the resulting solutions exhibit non-physical oscillations. The upwind difference approximations are computationally stable, although only first-order accurate, and the resulting solutions exhibit the effects of artificial viscosity. In addition, recent studies by Brandt and Yanvneh [2], and Zhang [3] indicate that the first-order upwind and the second-order central difference approximations may yield unreliable computational results for some convection-dominated flow problems. The second-order upwind FD approximations suffer from similar problems and the higher-order FD approximations of conventional type are computationally inefficient. In the context of higher-order FDs, compact FD schemes have good numerical stability and efficiency, and offer two attractive features: higher-order accuracy and small stencil. Consequently the number of numerical boundary conditions needed is considerably reduced, compared with conventional type higher-order methods. This is of great importance for the computation of various viscous flow and heat transfer problems. In recent years high-order compact FD methods have generated renewed interest and a variety of specialized techniques have been developed, mainly for steady-state convection-diffusion type problems in 2D, and applied to the incompressible N–S equations, see References [4–12] and the references therein. Dennis and Hudson [4] developed a fourth-order compact nine-point scheme. This method is a two-dimensional version of the methods of exponential type and uses the Numerov approximation. They solved the problem of natural convection in a square cavity with two vertical sidewalls maintained at different temperatures and obtained results up to $Ra = 10^5$. In 1991, Gupta [5] applied his fourth-order compact formulation to the solution of the steady, 2D, incompressible N-S equations in stream function–vorticity form. This study was followed more recently by similar research by Spotz and Carey [6], and Li *et al.* [7]. For the driven square cavity problem, Gupta solved up to $Re = 2000$ (Re is the non-dimensional Reynolds number) using point-SOR and successive approximations. Spotz and Carey [6] solved up to $Re = 1000$ using the generalized minimal residual method and successive approximations. Li *et al.* [7] solved up to $Re = 7500$ using point-SOR, Newton's method. For the heat cavity problem, Choo and Schultz [9] also presented a fourth-order compact nine-point method which converged for both large Ra and small Pr. The method was simple to implement, for it can use SOR iteration.

In this paper we derive a fourth-order compact FD scheme on the nine-point 2D stencil for the stream function–vorticity formulation of the Navier–Stokes/Boussinesq equations governing the fluid flow and heat transfer. It is shown that the present scheme yields highly accurate numerical solutions while still allowing point-successive overrelaxation or point-successive underrelaxation iteration for both large Ra and small Pr.

The outline of the present paper is as follows. In the next section we first present the compact nine-point fourth-order scheme for the steady-state Navier–Stokes/Boussinesq equations for two-dimensional, incompressible fluid flow and heat transfer using the stream function–vorticity formulation. Then we test the new fourth-order compact schemes for the Navier–Stokes/Boussinesq equations with the exact solutions in Section 3. In Section 4, the model problem of a square heated cavity is described with detailed comparisons of our solutions with existing solutions in the literature.

2. NUMERICAL METHODS

The Navier–Stokes/Boussinesq equations representing the steady-state two-dimensional, incompressible fluid flow and heat transfer are given in stream function–vorticity form as

$$\psi_{xx} + \psi_{yy} = -\zeta \tag{1}$$

$$T_{xx} + T_{yy} = \psi_y T_x - \psi_x T_y \tag{2}$$

$$\zeta_{xx} + \zeta_{yy} = (1/Pr)(\psi_y \zeta_x - \psi_x \zeta_y) - RaT_x + f \tag{3}$$

where ψ, T and ζ represent the stream, temperature and vorticity functions, respectively, f is a prescribed forcing function. Equations (2) and (3) are the non-conservation forms.

In this section we formulate a compact fourth-order FD method that can solve Equations (1)–(3) with the novelty of 'genuine compactness', i.e. the compact scheme is strictly with in the nine-point stencil. Note that each of these equations is a special case of the following Poisson-type equation:

$$\Phi_{xx} + \Phi_{yy} = g \tag{4}$$

where $g = g(x, y)$. Note that $\Phi = \psi$ and $g = -\zeta$ in Equation (1); $\Phi = T$ and $g = \psi_y T_x - \psi_x T_y$ in Equation (2); $\Phi = \zeta$ and $g = (1/Pr)(\psi_y \zeta_x - \psi_x \zeta_y) - RaT_x + f$ in Equation (3).

To set up a compact FD scheme for (4), we use Figure 1 that denotes the placement of nine points. Assuming a uniform mesh in both x- and y-directions, we number the mesh points $(x, y), (x+h, y), (x, y+h), (x-h, y), (x, y-h), (x+h, y+h), (x-h, y+h), (x-h, y-h)$ and $(x+h, y-h)$ as 0,1,2,3,4,5,6,7 and 8, respectively, where h is the mesh size. In writing the FD approximations a single subscript 'j' denotes the corresponding function value at the mesh point numbered 'j'.

Following [13], the second derivative at the point (x, y), are approximated by

$$\Phi_{xx0} = \left[\left(1 + \frac{h^2}{12}\,\delta_x^2\right)^{-1} \delta_x^2\right] \Phi_0 + O(h^4) \tag{5}$$

$$\Phi_{yy0} = \left[\left(1 + \frac{h^2}{12}\,\delta_y^2\right)^{-1} \delta_y^2\right] \Phi_0 + O(h^4) \tag{6}$$

where δ_x^2 and δ_y^2 are defined as

$$\delta_x^2 \Phi_0 = \frac{\Phi_1 - 2\Phi_0 + \Phi_3}{h^2}, \quad \delta_y^2 \Phi_0 = \frac{\Phi_2 - 2\Phi_0 + \Phi_4}{h^2} \tag{7}$$

Substituting (5) and (6) into the left-hand side of Equation (4) yields

$$\left[\left(1 + \frac{h^2}{12}\,\delta_y^2\right)\delta_x^2\right] \Phi_0 + \left[\left(1 + \frac{h^2}{12}\,\delta_x^2\right)\delta_y^2\right] \Phi_0 = \left(1 + \frac{h^2}{12}\,\delta_x^2 + \frac{h^2}{12}\,\delta_y^2\right) g_0 + O(h^4) \tag{8}$$

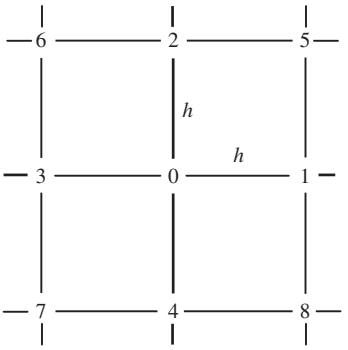

Figure 1. Computational stencil.

Using (7) in both sides of Equation (8), we get a fourth-order compact FD scheme for the Poisson-type equation given by (4)

$$\frac{1}{6h^2}\left(4\sum_{j=1}^{4}\Phi_j+\sum_{j=5}^{8}\Phi_j-20\Phi_0\right)=\frac{1}{12}\left(8g_0+\sum_{j=1}^{4}g_j\right) \tag{9}$$

Applying (7) to the left side of (8), and noting the use of

$$\delta_x^2 g_0 = g_{xx0}+O(h^2), \quad \delta_y^2 g_0 = g_{yy0}+O(h^2) \tag{10}$$

we can readily obtain another fourth-order compact FD scheme for the Poisson-type equation given by (4)

$$\frac{1}{6h^2}\left(4\sum_{j=1}^{4}\Phi_j+\sum_{j=5}^{8}\Phi_j-20\Phi_0\right)=g_0+\frac{h^2}{12}(g_{xx}+g_{yy})_0 \tag{11}$$

Now we are ready to set up the fourth-order FD schemes for each of the Equations (1)–(3). First, for Equation (1), where $\Phi=\psi$ and $g=-\zeta$, we have the following compact fourth-order FD scheme by (9)

$$\frac{1}{6h^2}\left(4\sum_{j=1}^{4}\psi_j+\sum_{j=5}^{8}\psi_j-20\psi_0\right)=-\frac{1}{12}\left(8\zeta_0+\sum_{j=1}^{4}\zeta_j\right) \tag{12}$$

Next, for Equation (2), where $\Phi=T$ and $g=\psi_y T_x-\psi_x T_y$, we have by (11):

$$\begin{aligned}&\frac{1}{6h^2}\left(4\sum_{j=1}^{4}T_j+\sum_{j=5}^{8}T_j-20T_0\right)\\&\quad=(\psi_y T_x-\psi_x T_y)_0+\frac{h^2}{12}\left[(\psi_y T_x-\psi_x T_y)_{xx}+(\psi_y T_x-\psi_x T_y)_{yy}\right]_0\end{aligned} \tag{13}$$

Straightforwardly calculating and using (2), we have

$$\begin{aligned}
&(\psi_y T_x - \psi_x T_y)_{xx} + (\psi_y T_x - \psi_x T_y)_{yy} \\
&\quad = T_x(\psi_{xx} + \psi_{yy})_y - T_y(\psi_{xx} + \psi_{yy})_x + \psi_y(T_{xx} + T_{yy})_x \\
&\qquad -\psi_x(T_{xx} + T_{yy})_y + 2\psi_{xy}(T_{xx} - T_{yy}) + 2T_{xy}(\psi_{yy} - \psi_{xx}) \\
&\quad = -T_x\zeta_y + T_y\zeta_x + \psi_y(\psi_y T_x - \psi_x T_y)_x - \psi_x(\psi_y T_x - \psi_x T_y)_y \\
&\qquad + 2\psi_{xy}(T_{xx} - T_{yy}) + 2T_{xy}(\psi_{yy} - \psi_{xx})
\end{aligned} \tag{14}$$

This result implies that $[(\psi_y T_x - \psi_x T_y)_{xx} + (\psi_y T_x - \psi_x T_y)_{yy}]_0$ in (13) is a combination of first and second derivatives of T and ψ, which can be approximated to a truncation error $O(h^2)$ by the 3×3 grid points. That is, $[(\psi_y T_x - \psi_x T_y)_{xx} + (\psi_y T_x - \psi_x T_y)_{yy}]_0$ can be approximated by T_j, ψ_j, $0 \leqslant j \leqslant 8$, giving a truncation error of order $O(h^2)$. We now consider the term $(\psi_y T_x - \psi_x T_y)_0$. For a fully fourth-order FD we need to approximate ψ_x, ψ_y, T_x and T_y with $O(h^4)$ accuracy, which is done as follows:

$$\frac{\psi_2 - \psi_4}{2h} = (\psi_y)_0 + \frac{h^2}{6}(\psi_{yyy})_0 + O(h^4) \tag{15}$$

$$\frac{\psi_1 - \psi_3}{2h} = (\psi_x)_0 + \frac{h^2}{6}(\psi_{xxx})_0 + O(h^4) \tag{16}$$

The above results, together with similar ones for T, yield

$$\begin{aligned}
(\psi_y T_x - \psi_x T_y)_0 = &\frac{1}{4h^2}[(\psi_2 - \psi_4)(T_1 - T_3) - (\psi_1 - \psi_3)(T_2 - T_4)] \\
&- \frac{h^2}{6}(\psi_y T_{xxx} - \psi_x T_{yyy} + T_x\psi_{yyy} - T_y\psi_{xxx})_0 + O(h^4)
\end{aligned} \tag{17}$$

To avoid extra points outside the (3×3)-point domain being required, we observe that

$$\begin{aligned}
&\psi_y T_{xxx} - \psi_x T_{yyy} + T_x\psi_{yyy} - T_y\psi_{xxx} \\
&\quad = \psi_y(T_{xx} + T_{yy})_x - \psi_y T_{xyy} - \psi_x(T_{xx} + T_{yy})_y + \psi_x T_{xxy} - T_x(\psi_{xxy} + \zeta_y) + T_y(\psi_{xyy} + \zeta_x) \\
&\quad = \psi_y(\psi_y T_x - \psi_x T_y)_x - \psi_x(\psi_y T_x - \psi_x T_y)_y - \psi_y T_{xyy} + \psi_x T_{xxy} \\
&\qquad - T_x\psi_{xxy} + T_y\psi_{xyy} - T_x\zeta_y + T_y\zeta_x
\end{aligned} \tag{18}$$

Combining (17) and (18) gives

$$(\psi_y T_x - \psi_x T_y)_0 = \frac{1}{4h^2}[(\psi_2 - \psi_4)(T_1 - T_3) - (\psi_1 - \psi_3)(T_2 - T_4)]$$

$$-\frac{h^2}{6}[\psi_y T_x - \psi_x T_y)_x - \psi_x(\psi_y T_x - \psi_x T_y)_y - \psi_y T_{xyy} + \psi_x T_{xxy}$$
$$-T_x\psi_{xxy} + T_y\psi_{xyy} - T_x\zeta_y + T_y\zeta_x]_0 + O(h^4)$$

The above results together with (14), yields

$$\frac{1}{6h^2}\left(4\sum_{j=1}^{4} T_j + \sum_{j=5}^{8} T_j - 20T_0\right)$$
$$= \frac{1}{4h^2}[(\psi_2 - \psi_4)(T_1 - T_3) - (\psi_1 - \psi_3)(T_2 - T_4)]$$
$$+ \frac{h^2}{12}[(\psi_x\psi_{yy}T_x + \psi_y\psi_{xx}T_y + 2\psi_x\psi_y T_{xy} - \psi_x\psi_{xy}T_y - \psi_y\psi_{xy}T_x - \psi_x^2 T_{yy} - \psi_y^2 T_{xx})$$
$$+ 2(\psi_y T_{xyy} - \psi_x T_{xxy} + \psi_{xxy}T_x - \psi_{xyy}T_y) + \zeta_y T_x - \zeta_x T_y$$
$$+ 2\psi_{xy}(T_{xx} - T_{yy}) + 2(\psi_{yy} - \psi_{xx})T_{xy}]_0 + O(h^4) \tag{19}$$

It is clear that all derivatives of ψ, T and ζ in (19) can be approximated up to $O(h^2)$ with the nine-point stencil. We derive a series of second-order difference formulas by Taylor series expansions, such as

$$u_{xx} = \frac{u_1 - 2u_0 + u_3}{h^2} + O(h^2), \quad u_{xy} = \frac{u_5 - u_6 + u_7 - u_8}{4h^2} + O(h^2) \tag{20}$$

$$u_x = \frac{u_1 - u_3}{2h} + O(h^2), \quad u_{xxy} = \frac{u_5 + u_6 - u_7 - u_8 - 2(u_2 - u_4)}{2h^3} + +O(h^2) \tag{21}$$

Applying (20) and (21) to (19) and using (13), and rearranging (13), we obtain the following fourth-order compact scheme for Equation (2):

$$\sum_{j=0}^{8} A_j T_j = 0 \tag{22}$$

$$A_0 = -40 - \tfrac{1}{2}[(\psi_1 - \psi_3)^2 + (\psi_2 - \psi_4)^2] \tag{23}$$

$$A_1 = 8 - (\psi_2 - \psi_4 + \psi_5 - \psi_8) - \tfrac{1}{4}[(\psi_1 - \psi_3)(\psi_2 - 2\psi_0 + \psi_4)$$
$$-\tfrac{1}{4}(\psi_2 - \psi_4)(\psi_5 - \psi_6 + \psi_7 - \psi_8) - (\psi_2 - \psi_4)^2 + h^2(\zeta_2 - \zeta_4)] \tag{24}$$

$$A_2 = 8 - (-\psi_1 + \psi_3 - \psi_5 + \psi_6) - \tfrac{1}{4}[(\psi_2 - \psi_4)(\psi_1 - 2\psi_0 + \psi_3)$$
$$-\tfrac{1}{4}(\psi_1 - \psi_3)(\psi_5 - \psi_6 + \psi_7 - \psi_8) - (\psi_1 - \psi_3)^2 - h^2(\zeta_1 - \zeta_3)] \tag{25}$$

$$A_3 = 8 - (-\psi_2 + \psi_4 - \psi_6 + \psi_7) - \tfrac{1}{4}[(-\psi_1 + \psi_3)(\psi_2 - 2\psi_0 + \psi_4)$$
$$+\tfrac{1}{4}(\psi_2 - \psi_4)(\psi_5 - \psi_6 + \psi_7 - \psi_8) - (\psi_2 - \psi_4)^2 - h^2(\zeta_2 - \zeta_4)] \tag{26}$$

$$A_4 = 8 - (\psi_1 - \psi_3 - \psi_7 + \psi_8) - \tfrac{1}{4}[(-\psi_2 + \psi_4)(\psi_1 - 2\psi_0 + \psi_3) + \tfrac{1}{4}(\psi_1 - \psi_3)(\psi_5 - \psi_6 + \psi_7 - \psi_8) - (\psi_1 - \psi_3)^2 + h^2(\zeta_1 - \zeta_3)] \tag{27}$$

$$A_5 = 2 - (-\psi_1 + \psi_2) - \tfrac{1}{8}(\psi_1 - \psi_3)(\psi_2 - \psi_4) \tag{28}$$

$$A_6 = 2 - (-\psi_2 + \psi_3) + \tfrac{1}{8}(\psi_1 - \psi_3)(\psi_2 - \psi_4) \tag{29}$$

$$A_7 = 2 - (-\psi_3 + \psi_4) - \tfrac{1}{8}(\psi_1 - \psi_3)(\psi_2 - \psi_4) \tag{30}$$

$$A_8 = 2 - (-\psi_4 + \psi_1) + \tfrac{1}{8}(\psi_1 - \psi_3)(\psi_2 - \psi_4) \tag{31}$$

Finally, for Equation (3), in which $\Phi = \zeta$ and $g = (1/Pr)(\psi_y\zeta_x - \psi_x\zeta_y) - RaT_x + f$, we have by (11):

$$\begin{aligned}
&\frac{1}{6h^2}\left(4\sum_{j=1}^{4}\zeta_j + \sum_{j=5}^{8}\zeta_j - 20\zeta_0\right) \\
&\quad = (1/Pr)\left\{(\psi_y\zeta_x - \psi_x\zeta_y) + \frac{h^2}{12}[(\psi_y\zeta_x - \psi_x\zeta_y)_{xx} + (\psi_y\zeta_x - \psi_x\zeta_y)_{yy}]\right\}_0 \\
&\qquad - Ra\left\{T_x + \frac{h^2}{12}[(T_x)_{xx} + (T_x)_{yy}]\right\}_0 + f_0 + \frac{h^2}{12}(f_{xx} + f_{yy})_0 \\
&\quad = J_1 + \frac{h^2}{12}J_2 + f_0 + \frac{h^2}{12}(f_{xx} + f_{yy})_0
\end{aligned} \tag{32}$$

where $J_1 = (1/Pr)(\psi_y\zeta_x - \psi_x\zeta_y)_0 - Ra(T_x)_0$ and $J_2 = (1/Pr)[(\psi_y\zeta_x - \psi_x\zeta_y)_{xx} + (\psi_y\zeta_x - \psi_x\zeta_y)_{yy}]_0 - Ra[(T_x)_{xx} + (T_x)_{yy}]_0$. Straightforwardly calculating and using (3) and (2), we have

$$\begin{aligned}
&(\psi_y\zeta_x - \psi_x\zeta_y)_{xx} + (\psi_y\zeta_x - \psi_x\zeta_y)_{yy} \\
&\quad = \zeta_x(\psi_{xx} + \psi_{yy})_y - \zeta_y(\psi_{xx} + \psi_{yy})_x + \psi_y(\zeta_{xx} + \zeta_{yy})_x - \psi_x(\zeta_{xx} + \zeta_{yy})_y \\
&\qquad + 2\psi_{xy}(\zeta_{xx} - \zeta_{yy}) + 2\zeta_{xy}(\psi_{yy} - \psi_{xx}) \\
&\quad = (1/Pr)\psi_y(\psi_y\zeta_x - \psi_x\zeta_y)_x - (1/Pr)\psi_x(\psi_y\zeta_x - \psi_x\zeta_y)_y - Ra(\psi_y T_{xx} - \psi_x T_{xy}) \\
&\qquad + (\psi_y f_x - \psi_x f_y) + 2\psi_{xy}(\zeta_{xx} - \zeta_{yy}) + 2\zeta_{xy}(\psi_{yy} - \psi_{xx})
\end{aligned} \tag{33}$$

$$\begin{aligned}
(T_x)_{xx} + (T_x)_{yy} &= (T_{xx} + T_{yy})_x \\
&= (\psi_y T_x - \psi_x T_y)_x \\
&= \psi_y T_{xx} - \psi_x T_{xy} + \psi_{xy} T_x - \psi_{xx} T_y
\end{aligned} \tag{34}$$

These results imply that J_2 in (32) is a combination of first and second derivatives of T, ζ and ψ, which can be approximated to a truncation error $O(h^2)$ by the 3×3 grid points. That

is, J_2 can be approximated by T_j, ζ_j and $\psi_j, 0 \leqslant j \leqslant 8$, giving a truncation error of order $O(h^2)$. We now consider the term J_1. Notice that (15) and (16), together with similar ones for ζ and T, yield

$$(\psi_y\zeta_x - \psi_x\zeta_y)_0 = \frac{1}{4h^2}[(\psi_2 - \psi_4)(\zeta_1 - \zeta_3) - (\psi_1 - \psi_3)(\zeta_2 - \zeta_4)] - \frac{h^2}{6}(\psi_y\zeta_{xxx} - \psi_x\zeta_{yyy} + \psi_{yyy}\zeta_x - \psi_{xxx}\zeta_y)_0 + O(h^4) \tag{35}$$

$$(T_x)_0 = \frac{T_1 - T_3}{2h} - \frac{h^2}{6}(T_{xxx})_0 + O(h^4) \tag{36}$$

To avoid extra points outside the (3×3)-point domain being required, we observe that

$$\begin{aligned}
&\psi_y\zeta_{xxx} - \psi_x\zeta_{yyy} + \zeta_x\psi_{yyy} - \zeta_y\psi_{xxx} \\
&\quad = \psi_y(\zeta_{xx} + \zeta_{yy})_x - \psi_y\zeta_{xyy} - \psi_x(\zeta_{xx} + \zeta_{yy})_y + \psi_x\zeta_{xxy} - \zeta_x(\psi_{xxy} + \zeta_y) + \zeta_y(\psi_{xyy} + \zeta_x) \\
&\quad = (1/Pr)\psi_y(\psi_y\zeta_x - \psi_x\zeta_y)_x - (1/Pr)\psi_x(\psi_y\zeta_x - \psi_x\zeta_y)_y - Ra(\psi_y T_{xx} - \psi_x T_{xy}) \\
&\qquad + (\psi_y f_x - \psi_x f_y) - \psi_y\zeta_{xyy} + \psi_x\zeta_{xxy} - \zeta_x\psi_{xxy} + \zeta_y\psi_{xyy}
\end{aligned} \tag{37}$$

$$\begin{aligned}
T_{xxx} &= (\psi_y T_x - \psi_x T_y - T_{yy})_x \\
&= \psi_y T_{xx} - \psi_x T_{xy} + \psi_{xy} T_x - \psi_{xx} T_y - T_{yyx}
\end{aligned} \tag{38}$$

Combining (33), (35) and (37) gives

$$\begin{aligned}
&\left\{(\psi_y\zeta_x - \psi_x\zeta_y) + \frac{h^2}{12}[(\psi_y\zeta_x - \psi_x\zeta_y)_{xx} + (\psi_y\zeta_x - \psi_x\zeta_y)_{yy}]\right\}_0 \\
&\quad = [(\psi_2 - \psi_4)(\zeta_1 - \zeta_3) - (\psi_1 - \psi_3)(\zeta_2 - \zeta_4)]/(4h^2) \\
&\qquad + \frac{h^2}{12}[(1/Pr)(\psi_x\psi_{yy}\zeta_x + \psi_y\psi_{xx}\zeta_y + 2\psi_x\psi_y\zeta_{xy} - \psi_x\psi_{xy}\zeta_y - \psi_y\psi_{xy}\zeta_x - \psi_x^2\zeta_{yy} - \psi_y^2\zeta_{xx}) \\
&\qquad + Ra(\psi_y T_{xx} - \psi_x T_{xy}) - (\psi_y f_x - \psi_x f_y) + 2\psi_{xy}(\zeta_{xx} - \zeta_{yy}) + 2(\psi_{yy} - \psi_{xx})\zeta_{xy} \\
&\qquad + 2(\psi_y\zeta_{xyy} - \psi_x\zeta_{xxy} + \psi_{xxy}\zeta_x - \psi_{xyy}\zeta_y)]_0
\end{aligned} \tag{39}$$

Combining (34), (36) and (38), we have

$$\begin{aligned}
&\left\{T_x + \frac{h^2}{12}[(T_x)_{xx} + (T_x)_{yy}]\right\}_0 \\
&\quad = \frac{T_1 - T_3}{2h} - \frac{h^2}{12}(\psi_y T_{xx} - \psi_x T_{xy} + \psi_{xy} T_x - \psi_{xx} T_y - 2T_{xyy})_0
\end{aligned} \tag{40}$$

The above result together with (32), yields

$$\begin{aligned}
&\frac{1}{6h^2}\left(4\sum_{j=1}^{4}\zeta_j+\sum_{j=5}^{8}\zeta_j-20\zeta_0\right)\\
&\quad=(1/Pr)\left\{\frac{1}{4h^2}[(\psi_2-\psi_4)(\zeta_1-\zeta_3)-(\psi_1-\psi_3)(\zeta_2-\zeta_4)]\right.\\
&\qquad+\frac{h^2}{12}[(1/Pr)(\psi_x\psi_{yy}\zeta_x+\psi_y\psi_{xx}\zeta_y+2\psi_x\psi_y\zeta_{xy}-\psi_x\psi_{xy}\zeta_y-\psi_y\psi_{xy}\zeta_x-\psi_x^2\zeta_{yy}-\psi_y^2\zeta_{xx})\\
&\qquad+Ra(\psi_yT_{xx}-\psi_xT_{xy})+2\psi_{xy}(\zeta_{xx}-\zeta_{yy})+2(\psi_{yy}-\psi_{xx})\zeta_{xy}\\
&\qquad\left.+2(\psi_y\zeta_{xyy}-\psi_x\zeta_{xxy}+\psi_{xxy}\zeta_x-\psi_{xyy}\zeta_y)]_0\right\}\\
&\qquad-Ra\frac{T_1-T_3}{2h}+Ra\frac{h^2}{12}(\psi_yT_{xx}-\psi_xT_{xy}+\psi_{xy}T_x-\psi_{xx}T_y-2T_{xyy})_0\\
&\qquad+f_0+\frac{h^2}{12}\{[(-1/Pr)\psi_y]f_x+[(1/Pr)\psi_x]f_y+f_{xx}+f_{yy}\}_0+O(h^4)
\end{aligned}\tag{41}$$

It is clear that all derivatives of ψ and ζ in (41) can be approximated up to $O(h^2)$ with the nine-point stencil.

Applying the difference formulas (20) and (21) to (41) and using (32), and rearranging (32), we obtain the following fourth-order compact scheme for Equation (3):

$$\begin{aligned}
\frac{1}{12h^2}\sum_{j=0}^{8}B_j\zeta_j&=-Ra\frac{T_1-T_3}{2h}+Ra\frac{h^2}{12}(\psi_yT_{xx}-\psi_xT_{xy}+\psi_{xy}T_x-\psi_{xx}T_y-2T_{xyy})_0\\
&\quad-Ra\frac{h^2}{12}[(-1/Pr)\psi_yT_{xx}+(1/Pr)\psi_xT_{xy}]_0\\
&\quad+f_0+\frac{h^2}{12}[(-1/Pr)\psi_yf_x+(1/Pr)\psi_xf_y+f_{xx}+f_{yy}]_0
\end{aligned}\tag{42}$$

$$B_0=-40-\frac{1}{2Pr^2}[(\psi_1-\psi_3)^2+(\psi_2-\psi_4)^2]\tag{43}$$

$$\begin{aligned}
B_1&=8-\frac{1}{Pr}(\psi_2-\psi_4+\psi_5-\psi_8)-\frac{1}{4}\frac{1}{Pr^2}[(\psi_1-\psi_3)(\psi_2-2\psi_0+\psi_4)\\
&\quad-\frac{1}{4}(\psi_2-\psi_4)(\psi_5-\psi_6+\psi_7-\psi_8)-(\psi_2-\psi_4)^2]
\end{aligned}\tag{44}$$

$$\begin{aligned}
B_2&=8-\frac{1}{Pr}(-\psi_1+\psi_3-\psi_5-\psi_6)-\frac{1}{4}\frac{1}{Pr^2}[(\psi_2-\psi_4)(\psi_1-2\psi_0+\psi_3)\\
&\quad-\frac{1}{4}(\psi_1-\psi_3)(\psi_5-\psi_6+\psi_7-\psi_8)-(\psi_1-\psi_3)^2]
\end{aligned}\tag{45}$$

$$\begin{aligned}
B_3&=8-\frac{1}{Pr}(-\psi_2+\psi_4-\psi_6+\psi_7)-\frac{1}{4}\frac{1}{Pr^2}[(-\psi_1+\psi_3)(\psi_2-2\psi_0+\psi_4)\\
&\quad+\frac{1}{4}(\psi_2-\psi_4)(\psi_5-\psi_6+\psi_7-\psi_8)-(\psi_2-\psi_4)^2]
\end{aligned}\tag{46}$$

$$B_4 = 8 - \frac{1}{Pr}(\psi_1 - \psi_3 - \psi_7 + \psi_8) - \frac{1}{4}\frac{1}{Pr^2}[(-\psi_2 + \psi_4)(\psi_1 - 2\psi_0 + \psi_3) + \frac{1}{4}(\psi_1 - \psi_3)(\psi_5 - \psi_6 + \psi_7 - \psi_8) - (\psi_1 - \psi_3)^2] \tag{47}$$

$$B_5 = 2 - \frac{1}{Pr}(-\psi_1 + \psi_2) - \frac{1}{8}\frac{1}{Pr^2}(\psi_1 - \psi_3)(\psi_2 - \psi_4) \tag{48}$$

$$B_6 = 2 - \frac{1}{Pr}(-\psi_2 + \psi_3) + \frac{1}{8}\frac{1}{Pr^2}(\psi_1 - \psi_3)(\psi_2 - \psi_4) \tag{49}$$

$$B_7 = 2 - \frac{1}{Pr}(-\psi_3 + \psi_4) - \frac{1}{8}\frac{1}{Pr^2}(\psi_1 - \psi_3)(\psi_2 - \psi_4) \tag{50}$$

$$B_8 = 2 - \frac{1}{Pr}(-\psi_4 + \psi_1) + \frac{1}{8}\frac{1}{Pr^2}(\psi_1 - \psi_3)(\psi_2 - \psi_4) \tag{51}$$

In (42), all derivatives of T can be approximated with $O(h^2)$ on the nine-point stencil. Thus, we have a fully fourth-order compact scheme for Equation (3).

The new fourth-order compact schemes (12), (22) and (42) are to be solved by a point-SOR/ successive underrelaxation method.

3. NAVIER–STOKES/BOUSSINESQ EQUATIONS WITH EXACT SOLUTION

In this section we obtain numerical solutions of (1), (2) and (3) using the new fourth-order compact scheme (12), (22) and (42). The test problem used is chosen such that the analytical solution is available, so a rigorous comparison can be made.

To construct a test problem with known solution we specify the temperature and the stream function

$$T = x + y, \quad \psi = 1/Pr\, e^{x+y}$$

on the unit square. The corresponding vorticity function, derived from (1), is

$$\zeta = -2/Pr\, e^{x+y}$$

and the forcing function, derived from (3), is

$$f = Ra - 4/Pr\, e^{x+y}$$

We notice that the above solution is smooth in the unit square.

We consider the test problem with Dirichlet boundary conditions, i.e. boundary values of ψ, T and ζ are given. Various Rayleigh numbers ranging from $Ra = 10^2$ to 10^4 and Prandtl numbers $0.01 \leqslant Pr \leqslant 1$ were tested. Tables I–III show RMS (root-mean-square) errors err_1 and err_2, which were obtained from the grid system having $(N_1+1)\times(N_1+1)$ and $(N_2+1)\times(N_2+1)$ points, respectively. With these values, the resulting rate of convergence was estimated in the unit square for stream function, vorticity and temperature. The rate of convergence is defined below:

$$\mathrm{rate} = \frac{\log(\mathrm{err}_1/\mathrm{err}_2)}{\log(N_1/N_2)}$$

Table I. RMS errors with the rate of convergence in $(0,1) \times (0,1)$ for stream function, vorticity and temperature at $Ra = 10^2$ and $Pr = 1$.

Grid	ζ-error	Rate	ψ-error	Rate	T-error	Rate
6×6	3.436(−4)	—	1.408(−5)	—	2.752(−5)	—
11×11	1.907(−5)	4.17	7.577(−7)	4.22	1.567(−6)	4.13
21×21	1.123(−6)	4.09	4.472(−8)	4.08	9.297(−8)	4.07
41×41	6.826(−8)	4.04	2.731(−9)	4.03	5.660(−9)	4.04

Note: $3.436(-4) = 3.436 \times 10^{-4}$, etc.

Table II. RMS errors with the rate of convergence in $(0,1) \times (0,1)$ for stream function, vorticity and temperature at $Ra = 10^4$ and $Pr = 1$.

Grid	ζ-error	Rate	ψ-error	Rate	T-error	Rate
6×6	1.465(−2)	—	5.554(−4)	—	3.576(−5)	—
11×11	9.351(−4)	3.97	3.308(−5)	4.07	2.049(−6)	4.13
21×21	5.584(−5)	4.07	1.956(−6)	4.08	1.210(−7)	4.08
41×41	3.402(−6)	4.04	1.192(−7)	4.04	7.367(−9)	4.04

Table III. RMS errors with the rate of convergence in $(0,1) \times (0,1)$ for stream function, vorticity and temperature at $Ra = 10^2$ and $Pr = 10^{-2}$.

Grid	ζ-error	Rate	ψ-error	Rate	T-error	Rate
21×21	7.599(−7)	—	7.970(−7)	—	2.543(−5)	—
31×31	1.475(−7)	4.04	7.706(−8)	4.04	5.618(−6)	3.73
41×41	4.622(−8)	4.03	2.418(−8)	4.03	1.844(−6)	3.87

It is observed that the convergence rates for the h^4 scheme, (12), (22) and (42), are four. This confirms that the compact scheme (12), (22) and (42) is of fourth-order accuracy when the solutions of (1), (2) and (3) are smooth. This test problem is solved by the point-SOR iteration method.

4. HEATED CAVITY PROBLEM

As a model problem we consider a square cavity ($0 \leqslant x \leqslant 1, 0 \leqslant y \leqslant 1$) with differentially heated vertical (left and right) walls and adiabatic horizontal (top and bottom) walls (see Figure 2), which is one of the classical problems in the field of heat transfer. The boundary conditions for the present problem can be specified as follows:

$$\psi = 0, \quad \psi_x = 0, \quad T = 1 \tag{52}$$

on the hot wall,

$$\psi = 0, \quad \psi_x = 0, \quad T = 0 \tag{53}$$

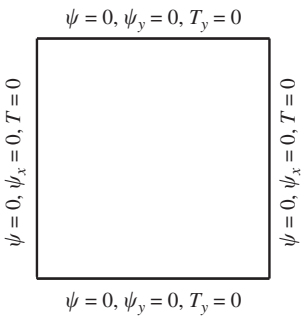

Figure 2.

on the cold wall, and

$$\psi = 0, \quad \psi_y = 0, \quad T_y = 0 \tag{54}$$

on the top and bottom walls.

In particular, the above model problem has been frequently used as a test problem for assessing the performance of numerical solution techniques. A comprehensive comparison paper concerning the numerical solutions on this problem was published by de Vahl Davis and Jones [15]. They summarized numerical results from 37 sources for the case of $Pr = 0.71$ with Ra ranging from 10^3 to 10^6. The results of various contributions were compared with benchmark solutions proposed by de Vahl Davis [16], who formulated the problem in terms of stream-function and vorticity and used a finite difference technique, along with grid refinement (up to 81×81 points) and extrapolation procedures. As regards more recent work on this topic, some studies that are particularly worth mentioning are those of Choo and Schultz [9], Hortmann *et al.* [17], Le Quéré [18], and Syrjälä [19].

4.1. High-order numerical boundary conditions

The implementation of numerical boundary conditions has received considerable attention in the past. In the previous section, we formulated the high-order compact difference method for given Equations (1)–(3). In this section, we shall present high-order formulas for the heated cavity problem on and near the boundary.

For the case $T_y = 0$ on the side boundaries, if we use the formula

$$T_y|_0 = (-2T_{-1} - 3T_0 + 6T_1 - T_2)/(\pm 6h) + O(h^3) \tag{55}$$

where the notation in Figure 3 is used, and solve $T_y|_0 = 0$ for T_{-1}, we obtain the temperature on the outer boundary

$$T_{-1} = (-3T_0 + 6T_1 - T_2)/2 + O(h^4) \tag{56}$$

To prevent numerical instability, it is necessary to give an inner boundary on the stream function equation. (The term 'inner boundary' denotes the set of all points that lie at a distance h from the boundary.) We reason that this is because it forces the derivative condition in (52),

Figure 3.

(53) and (54) to be satisfied. Using Taylor series, we can write

$$\begin{aligned}\psi_1 + \alpha\psi_2 + \beta\psi_3 = {} & (1+\alpha+\beta)\psi_0 + (1+2\alpha+3\beta)h\psi_{\mathrm{no}} \\ & + (1+4\alpha+9\beta)h^2/2\psi_{\mathrm{nno}} + (1+8\alpha+27\beta)h^3/6\psi_{\mathrm{nnno}} \\ & + (1+16\alpha+81\beta)h^4/24\psi_{\mathrm{nnnno}} + O(h^5)\end{aligned} \tag{57}$$

Here, ψ_{no} represents the derivative of ψ in the direction normal to the wall at the wall. We choose

$$1+8\alpha+27\beta=0, \quad 1+16\alpha+81\beta=0 \tag{58}$$

to cancel the h^3 and h^4 terms, to yield

$$\psi_1 + \alpha\psi_2 + \beta\psi_3 = (1+\alpha+\beta)\psi_0 + (1+2\alpha+3\beta)h\psi_{\mathrm{no}} + (1+4\alpha+9\beta)h^2/2\psi_{\mathrm{nno}} + O(h^5) \tag{59}$$

Solving linear system (58), we obtain

$$\alpha = -\tfrac{1}{4}, \quad \beta = \tfrac{1}{27} \tag{60}$$

Substituting (60) into (59), and using Equations (52), (53), (54) and (1), yields

$$\psi_1 = (1/4)\psi_2 - (1/27)\psi_3 - (h^2/6)\zeta_0 \tag{61}$$

Since there is no explicit boundary condition for ζ, we need to update boundary vorticities. Using Taylor series, we have

$$\begin{aligned}\psi_1 + \gamma\psi_2 = {} & (1+\gamma)\psi_0 + h(1+2\gamma)\psi_{\mathrm{no}} + (h^2/2)(1+4\gamma)\psi_{\mathrm{nno}} + (h^3/6)(1+8\gamma)\psi_{\mathrm{nnno}} \\ & + (h^4/24)(1+16\gamma)\psi_{\mathrm{nnnno}} + O(h^5)\end{aligned} \tag{62}$$

Using (1), ψ_{nn} in (62) can be written as

$$\begin{aligned}\psi_{\mathrm{nno}} &= -\zeta_0 - \psi_{ss0} \\ &= -\zeta_0\end{aligned} \tag{63}$$

where we have used the fact that $\psi_{ss0}=0$ on a wall (s is the local direction tangent to on the boundaries). Furthermore, differentiating (63),

$$\begin{aligned}\psi_{\mathrm{nnno}} &= -\zeta_{\mathrm{no}} - \psi_{\mathrm{ssno}} \\ &= -\zeta_{\mathrm{no}}\end{aligned} \tag{64}$$

Substituting (63) and (64) into (62), and setting $\gamma = -\frac{1}{16}$ and using Equations (52), (53), (54) and (1) again to substitute for the first and second derivatives, gives

$$16\psi_1 - \psi_2 = -6h^2\zeta_0 - (4h^3/3)\zeta_{\mathrm{no}} + O(h^5) \tag{65}$$

Thus, if we use

$$\zeta_{\mathrm{no}} = (-3\zeta_0 + 4\zeta_1 - \zeta_2)/(2h) + O(h^2) \tag{66}$$

to substitute for ζ_{no}, the resulting high-order formula is

$$(h/21)(6\zeta_0 + 4\zeta_1 - \zeta_2) + O(h^4) = (-16\psi_1 + \psi_2)/(14h) \tag{67}$$

This expression is fourth-order-accurate [14], while using only three grid points for ψ and ζ.

Various high-order approximations were tried in place of (56), (61) and (67). However, the approximation (56), (61) and (67) gave the best overall results. The differences between results for the various approximations could be made negligible by using a small enough h.

4.2. Finite difference algorithm

The finite difference algorithm is now briefly outlined. Suppose $\psi^{(n)}$, $T^{(n)}$ and $\zeta^{(n)}$are known. The solution of the discrete Navier–Stokes/Boussinesq equations (12), (22) and (42) is obtained by the following iterative procedure:

1. Solution of the stream-function equation (12)
   (a) Determine inner boundaries on the stream function equation from (61):

$$\psi_1^{(n+1)} = (1/4)\psi_2^{(n)} - (1/27)\psi_3^{(n)} - (h^2/6)\zeta_0^{(n)} \tag{68}$$

   where the notation in Figure 3 is used.
   (b) In region $[2h, 1-2h]\times[2h, 1-2h]$, solve the stream function equation (12) to obtain $\psi^{(n+1)}$ from:

$$\frac{1}{6h^2}\left(4\sum_{j=1}^{4}\psi_j^{(n+1)} + \sum_{j=5}^{8}\psi_j^{(n+1)} - 20\psi_0^{(n+1)}\right) = -\frac{1}{12}\left(8\zeta_0^{(n)} + \sum_{j=1}^{4}\zeta_j^{(n)}\right) \tag{69}$$

   where the notation in Figure 1 is used.
2. Solution of the temperature equation (22)
   (a) Determine the temperature $T_{-1}^{(n+1)}$ on the outer boundary from (56):

$$T_{-1}^{(n+1)} = (-3T_0^{(n)} + 6T_1^{(n)} - T_2^{(n)})/2 \tag{70}$$

   where the notation in Figure 3 is used.

(b) In region $[h, 1-h]\times[0,1]$, solve the temperature equation (22) to obtain $T^{(n+1)}$ from:

$$\sum_{j=0}^{8} A_j^{(n+1)} T_j^{(n+1)} = 0 \tag{71}$$

where the notation in Figure 1 is used, and A_j are determined by (23)–(31).

3. Solution of the vorticity equation (42)

(a) Determine the vorticity boundary $\zeta_0^{(n+1)}$ from (67):

$$(h/21)(6\zeta_0^{(n+1)} + 4\zeta_1^{(n)} - \zeta_2^{(n)}) = (-16\psi_1^{(n+1)} + \psi_2^{(n+1)}))/(14h) \tag{72}$$

where the notation in Figure 3 is used.

(b) In region $[h, 1-h]\times[h, 1-h]$, solve the vorticity equation (42) to obtain $\zeta^{(n+1)}$ from:

$$\begin{aligned}
&\frac{1}{12h^2}\sum_{j=0}^{8} B_j^{(n+1)}\zeta_j^{(n+1)} \\
&\quad = \left\{ -Ra\,\frac{T_1 - T_3}{2h} + Ra\,\frac{h^2}{12}\,(\psi_y T_{xx} - \psi_x T_{xy} + \psi_{xy} T_x - \psi_{xx} T_y - 2T_{xyy}) \right. \\
&\qquad \left. -Ra\,\frac{h^2}{12}\,[(-1/Pr)\psi_y T_{xx} + (1/Pr)\psi_x T_{xy}] \right\}_0^{(n+1)}
\end{aligned} \tag{73}$$

where the notation in Figure 1 is used, and B_j are determined by (43)–(51).

4. Repeat the steps 1 to 3 from $n = 0, 1, 2, \ldots$ until a certain convergence criterion is met.

The iterative steps 1 to 3 form an 'outer iteration'. If Equations (69) subject to the boundary conditions (68) are solved by an iterative procedure, then the step 1 is called an 'inner iteration' for ψ. Similarly, if Equations (71) or (73) subject to the boundary conditions are solved by an iterative procedure, then the steps 2, 3 are called inner iterations for T, ζ. The similar inner-outer iteration procedure has been described by Gupta and Manohar [20]. In the present work, we use one or more inner iterations for ψ, T and an inner iteration for ζ at each outer iteration.

4.3. Comparisons with existing solutions

In this section, converged solutions have been obtained for Prandtl numbers $Pr = 0.71$ with Ra ranging from 10^3 to 10^7. Results have been obtained for the number of grid spacing n in each direction varying from 20 to 160. All results were run on the Pentium/200. The time for $Ra = 10^5$ and $n = 20$ was 13.18 s, for $Ra = 10^5$ and $n = 40$ it was 1 min 12.66 s, for $Ra = 10^5$ and $n = 60$ it was 8 min 27.56 s, for $Ra = 10^5$ and $n = 80$ it was 16 min 48 s and for $Ra = 10^5$ and $n = 100$ it was 61 min 47.19 s. We used point-SOR or successive underrelaxation iteration with a root-mean-square (RMS) convergence test of 10^{-4}.

Tables IV–VIII contain results which are compared with those of de Vahl Davis [16], Dennis and Hudson [4], Chen *et al.* [8], Choo and Schultz [9], Hortmann and Perić [17], Le Quéré [18], and Syrjälä [19]. In each table, the following reference quantities were

Table IV. Comparison of the bench mark solution by de Vahl Davis [16], the compact difference solutions by Dennis and Hudson [4] and Chen *et al.* [8], and the stable fourth-order solutions by Choo and Schultz [9] ($Ra = 10^3, Pr = 0.71$).

First author	$\lvert\psi_{\text{mid}}\rvert$	$\lvert\psi\rvert_{\max}$	$u_{\max}$ $y(x=0.5)$	$v_{\max}$ $x(y=0.5)$	Nu_0	$Nu_{\max}$ $y(x=0)$	$Nu_{\min}$ $y(x=0)$
Present ($n=20$)	1.1742	1.1742	3.6488	3.6967	1.1174	1.5042	0.6920
			0.8133	0.1782		0.0928	1
Present ($n=30$)	1.1744	1.1744	3.6491	3.6969	1.1174	1.5053	0.6912
			0.8131	0.1785		0.0892	1
Present ($n=40$)	1.1744	1.1744	3.6489	3.6966	1.1175	1.5056	0.6911
			0.8133	0.1784		0.0889	1
Present ($n=50$)	1.1743	1.1743	3.6484	3.6962	1.1175	1.5057	0.6912
			0.8133	0.1784		0.0887	1
Present ($n=60$)	1.1741	1.1741	3.6481	3.6958	1.1176	1.5058	0.6912
			0.8133	0.1783		0.0886	1
De Vahl Davis [16]	1.174	n.a.	3.649	3.697	1.117	1.505	0.692
			0.813	0.178		0.092	1
Dennis *et al.* [4]	1.1747	n.a.	3.6497	3.6977	1.1176	1.5058	0.6913
			0.8132	0.1783		0.0871	1
Chen *et al.* [8]	1.1746	n.a.	3.6501	3.6980	1.1172	1.5055	0.6915
			0.8131	0.1784		0.0860	1
Choo *et al.* [9]	1.174	1.174	n.a.	n.a.	1.116	n.a.	n.a.
			n.a.	n.a.	n.a.		n.a.

n.a. =Not available.

considered:

$|\psi_{\text{mid}}|$: the absolute value of stream function in the midpoint of the cavity
$|\psi|_{\max}$: the maximum absolute value of stream function
$u_{\max}$: the maximum value of horizontal velocity component on the vertical midplane ($x=0.5$) of the cavity, together with its location
$v_{\max}$: the maximum value of vertical velocity component on the horizontal midplane ($y=0.5$) of the cavity, together with its location
Nu_0: the average Nusselt number Nu on the heated wall ($x=0$)
$Nu_{\max}$: the maximum values of the local Nusselt number on the heated side ($x=0$), together with their locations
$Nu_{\min}$: the minimum values of the local Nusselt number on the heated side ($x=0$), together with their locations

It is worth pointing out that in the present study the maximum values of the reference quantities and their locations were obtained by interpolation from the adjacent nodal values.

Following de Vahl Davis [16], we define the local Nusselt number at the hot wall ($x=0$) as

$$Nu = -(T_x)_{0,j} \tag{74}$$

From Equation (74), we obtain immediately the average values of the Nusselt number across the left boundary

$$Nu_0 = -\int_0^1 (T_x)_{0,j}\,\mathrm{d}y \tag{75}$$

Table V. Comparison of the bench mark solution by de Vahl Davis [16], the compact difference solutions by Dennis and Hudson [4] and Chen *et al.* [8], the stable fourth-order solutions by Choo and Schultz [9], the finite volume multigrid results by Hortmann and Peric [17], and the finite element solutions by Syrjälä [19] ($Ra = 10^4, Pr = 0.71$).

First author	$\lvert\psi_{\text{mid}}\rvert$	$\lvert\psi\rvert_{\max}$	$u_{\max}$	$v_{\max}$	Nu_0	$Nu_{\max}$	$Nu_{\min}$
Present ($n = 20$)	5.0759	5.0759	16.1979	19.6352	2.2408	3.5208	0.5863
			0.8232	0.1192		0.1454	1
Present ($n = 30$)	5.0748	5.0748	16.1876	19.6313	2.2426	3.5256	0.5847
			0.8232	0.1190		0.1452	1
Present ($n = 40$)	5.0743	5.0743	16.1849	19.6295	2.2434	3.5278	0.5846
			0.8233	0.1189		0.1449	1
Present ($n = 50$)	5.0740	5.0740	16.1840	19.6287	2.2439	3.5289	0.5846
			0.8232	0.1189		0.1446	1
Present ($n = 60$)	5.0738	5.0738	16.1837	19.6282	2.2441	3.5295	0.5847
			0.8233	0.1189		0.1445	1
De Vahl Davis [16]	5.071	n.a.	16.178	19.617	2.238	3.528	0.586
			0.823	0.119		0.143	1
Dennis [4]	5.0735	n.a.	16.1829	19.6293	2.2396	3.5193	0.5851
			0.8232	0.119		0.1440	1
Chen [8]	5.0735	n.a.	16.1809	19.6297	2.2361	3.5180	0.5855
			0.8233	0.1191		0.1435	1
Choo [9]	5.073	5.073	n.a.	n.a.	2.243	n.a.	n.a.
			n.a.	n.a.		n.a.	n.a.
Hortmann [17]	n.a.	n.a.	16.1759	19.6242	2.2447	3.5313	n.a.
			0.8255	0.1201		0.8540	n.a.
Syrjälä [19]	5.0737	n.a.	16.1834	19.6282	2.448	n.a.	n.a.
			0.8232	0.1189		n.a.	n.a.

As in Reference [16], the average values of Nusselt number was calculated through the use of Simpson's rule to approximation the integration in Equation (75). For an arbitrary node (x_0, y_j) along the vertical wall $x = 0$, the given $(T_x)_{0,j}$ is

$$\begin{aligned}(T_x)_{0j} = {} & (-15T_{0,j} + 16T_{1,j} - T_{2,j})/(14h) \\ & + [-3(T_{0,j+1} - 2T_{0,j} + T_{0,j-1}) + 4(T_{1,j+1} - 2T_{1,j} + T_{1,j-1}) \\ & - (T_{2,j+1} - 2T_{2,j} + T_{0,j-1})]/(21h) \end{aligned} \tag{76}$$

This expression is fourth-order-accurate, while using only three grid points for T (along the x-direction). A brief derivation of formula (76) is given in Appendix A.

All velocity field results are presented in terms of the stream function:

$$u = \psi_y, \quad v = -\psi_x \tag{77}$$

The velocities u, v at a grid point (x, y) are calculated from the discrete approximation of Equation (77). The following approximations are compact and have a local truncation error of order h^4 [13]:

$$u_2 + 4u_0 + u_4 = (\psi_y)_2 + 4(\psi_y)_0 + (\psi_y)_4 = 3(\psi_2 - \psi_4)/h \tag{78}$$

$$v_1 + 4v_0 + v_3 = (-\psi_x)_1 + 4(-\psi_x)_0 + (-\psi_x)_3 = -3(\psi_1 - \psi_3)/h \tag{79}$$

Table VI. Comparison of the bench mark solution by de Vahl Davis [16], the compact difference solutions by Dennis and Hudson [4] and Chen *et al.* [8], the stable fourth-order solutions by Choo and Schultz [9], the finite volume multigrid results by Hortmann and Perić [17], and the finite element solutions by Syrjälä [19] ($Ra = 10^5, Pr = 0.71$).

First author	$\lvert\psi_{\text{mid}}\rvert$	$\lvert\psi\rvert_{\max}$	$u_{\max}$	$v_{\max}$	Nu_0	$Nu_{\max}$	$Nu_{\min}$
Present ($n = 30$)	9.1152	9.6038	34.7640	68.6361	4.5112	7.6920	0.7315
			0.8546	0.0661		0.0808	1
Present ($n = 40$)	9.1159	9.6119	34.7495	68.6404	4.5156	7.6967	0.7284
			0.8549	0.0660		0.0827	1
Present ($n = 50$)	9.1162	9.6164	34.7450	68.6397	4.5177	7.7043	0.7276
			0.8547	0.0659		0.0829	1
Present ($n = 60$)	9.1162	9.6174	34.7428	68.6387	4.5189	7.7091	0.7275
			0.8546	0.0659		0.0828	1
Present ($n = 70$)	9.1161	9.6173	34.7417	68.6383	4.5195	7.7121	0.7275
			0.8546	0.0659		0.0827	1
De Vahl Davis [16]	9.111	9.612	34.73	68.59	4.509	7.717	0.729
			0.855	0.066		0.081	1
Dennis [4]	9.1126	n.a.	34.716	68.637	4.4959	7.6830	0.7279
			0.8545	0.0660		0.0800	1
Chen [8]	9.1105	n.a.	34.6977	68.7055	4.5220	7.8126	0.7278
			0.8550	0.0669		0.0801	1
Choo [9]	9.116	9.617	n.a.	n.a.	4.524	n.a.	n.a.
			n.a.	n.a.		n.a.	n.a.
Hortmann [17]	n.a.	n.a.	34.7385	68.6359	4.5219	7.7269	n.a.
			0.8554	0.0660		0.9177	n.a.
Syrjälä [19]	9.1156	n.a.	34.7406	68.6365	4.5216	n.a.	n.a.
			0.8546	0.0659		n.a.	n.a.

Tables IV–VIII compare the present results for $Ra = 10^3$, 10^4, 10^5, 10^6 and 10^7 with the benchmark solutions in de Vahl Davis [16], the compact difference solutions in Dennis and Hudson [4] and Chen *et al.* [8], the stable fourth-order difference solutions in Choo and Schultz [9], the finite-volume multigrids solutions in Hortmann and Perić [17], the results from Le Quéré [18], who solved the problems using a pseudo-spectral Chebyshev algorithm, and the finite element solutions in Syrjälä [19]. These tables show the excellent agreement of the present results with those of the benchmark solution and the stable fourth-order method for all the values of Ra from 10^3 to 10^6, with those of the compact difference method up to 10^5, with those of Le Quéré for $Ra = 10^6$ and 10^7, and with those of finite element method for $Ra = 10^5$ and 10^6.

Tables IV–VIII also show the convergence of the current compact fourth-order method as n increases (h decreases). Note that there is very little change in the results in Tables IV–VIII for $n = 40$, 50 and 60 for $Ra \leqslant 10^4$, and for $n = 50$, 60 and 70 for $Ra = 10^5$, and for $n = 80$, 100 and 120 for $Ra = 10^6$, showing excellent convergence. For $Ra = 10^7$ the results are quite close for $n = 120$, 140 and 160. Although the present method showed excellent convergence, a finer mesh size was needed for larger Ra to obtain accuracy. This limitation may be overcome by the use of mesh refinement or co-ordinate transformation, which is under consideration.

To obtain a clearer assessment of our $O(h^4)$ results, the percentage differences with respect to the reference quantities are also given in Table IX. The solutions of de Vahl Davis

Table VII. Comparison of the bench mark solution by de Vahl Davis [16], the compact difference solutions by Dennis and Hudson [4] and Chen *et al.* [8], the stable fourth-order solutions by Choo and Schultz [9], the finite volume multigrid results by Hortmann and Peric [17], the results from Le Quéré [8], and the finite element solutions by Syrjälä [19] ($Ra = 10^6, Pr = 0.71$).

First author	$\lvert\psi_{\text{mid}}\rvert$	$\lvert\psi\rvert_{\max}$	$u_{\max}$	$v_{\max}$	Nu_0	$Nu_{\max}$	$Nu_{\min}$
Present ($n = 40$)	16.3767	16.8015	65.0021	220.6320	8.7832	17.7970	0.9997
			0.8505	0.0380		0.0287	1
Present ($n = 60$)	16.3777	16.8028	64.8630	220.5371	8.8079	17.4795	0.9820
			0.8501	0.0378		0.0380	1
Present ($n = 80$)	16.3834	16.8082	64.8442	220.5616	8.8164	17.4784	0.9793
			0.8499	0.0378		0.0393	1
Present ($n = 100$)	16.3855	16.8101	64.8383	220.5668	8.8197	17.4962	0.9788
			0.8499	0.0377		0.0396	1
Present ($n = 120$)	16.3863	16.8107	64.8308	220.5675	8.8216	17.5087	0.9787
			0.8501	0.0377		0.0396	1
De Vahl Davis [16]	16.320	16.750	64.63	219.36	8.817	17.925	0.989
			0.850	0.037		0.037	1
Choo [9]	16.379	16.804	n.a.	n.a.	8.870	n.a.	n.a.
			n.a.	n.a.		n.a.	n.a.
Hortmann [17]	n.a.	n.a.	64.8340	220.473	8.8255	17.540	n.a.
			0.8504	0.0389		0.9610	n.a.
Le Quéré [18]	16.3864	16.8111	64.8344	220.559	8.8252	17.5360	0.9795
			0.850	0.038		0.0378	1
Syrjälä [19]	16.3863	n.a.	64.833	220.56	8.8251	n.a.	n.a.
			0.8500	0.0379		n.a.	n.a.

Table VIII. Comparison of the bench mark solutions from Le Quéré [18] and the finite element solutions by Syrjälä [19] ($Ra = 10^7, Pr = 0.71$).

First author	$\lvert\psi_{\text{mid}}\rvert$	$\lvert\psi\rvert_{\max}$	$u_{\max}$ $y(x = 0.5)$	$v_{\max}$ $x(y = 0.5)$	Nu_0	$Nu_{\max}$ $y(x = 0)$	$Nu_{\min}$ $y(x = 0)$
Present ($n = 80$)	29.3293	30.1295	148.5880	699.2687	16.4450	40.3369	1.3831
			0.8798	0.0214		0.0092	1
Present ($n = 100$)	29.3328	30.1183	148.5402	699.2121	16.4800	39.5059	1.3713
			0.8792	0.0213		0.0160	1
Present ($n = 120$)	29.3461	30.1371	148.5357	699.3002	16.4965	39.3380	1.3674
			0.8795	0.0213		0.0184	1
Present ($n = 140$)	29.3524	30.1549	148.5751	699.2764	16.5054	39.3230	1.3660
			0.8798	0.0213		0.0180	1
Present ($n = 160$)	29.3562	30.1553	148.5695	699.2991	16.5106	39.2540	1.3655
			0.8794	0.0213		0.0179	1
Le Quéré [18]	29.361	30.165	148.59	699.17	16.523	39.39	1.366
			0.879	0.021		0.018	1
Syrjälä [19]	29.3616	n.a.	148.593	699.506	16.5299	n.a.	n.a.
			0.8794	0.0213		n.a.	n.a.

[16] ($Ra = 10^3$–10^6) and Le Quéré [18] ($Ra = 10^6$ and 10^7) have been taken as references for comparison. De Vahl Davis [16] has estimated the percentage errors of his benchmark solutions for $Ra = 10^3$, 10^4, 10^5 and 10^6 are no more than 0.1, 0.2, 0.3 and 1.0. Results show

Table IX. Percentage differences with respect to the reference quantities.

Ra	h	$\lvert\psi_{\mathrm{mid}}\rvert$	$u_{\max}$	$v_{\max}$	Nu_0
	1/20	0.017	0.005	0.008	0.035
	1/30	0.034	0.002	0.002	0.035
10^3 [16]	1/40	0.034	0.002	0.010	0.044
	1/50	0.025	0.016	0.021	0.044
	1/60	0.008	0.024	0.032	0.053
	1/20	0.096	0.123	0.092	0.125
	1/30	0.074	0.059	0.072	0.205
10^4 [16]	1/40	0.065	0.042	0.063	0.241
	1/50	0.059	0.037	0.059	0.263
	1/60	0.055	0.035	0.057	0.272
	1/30	0.046	0.097	0.067	0.048
	1/40	0.053	0.056	0.073	0.146
10^5 [16]	1/50	0.057	0.043	0.072	0.192
	1/60	0.057	0.037	0.071	0.219
	1/70	0.055	0.035	0.070	0.232
	1/40	0.347	0.575	0.579	0.383
	1/60	0.353	0.360	0.536	0.103
10^6 [16]	1/80	0.388	0.331	0.547	0.006
	1/100	0.401	0.322	0.550	0.030
	1/120	0.406	0.310	0.550	0.052
	1/40	0.059	0.258	0.033	0.475
	1/60	0.053	0.044	0.009	0.196
10^6 [18]	1/80	0.018	0.015	0.001	0.099
	1/100	0.005	0.006	0.003	0.062
	1/120	0.000	0.005	0.003	0.040
	1/80	0.107	0.001	0.014	0.472
	1/100	0.096	0.033	0.006	0.260
10^7 [18]	1/120	0.050	0.036	0.018	0.160
	1/140	0.029	0.010	0.015	0.106
	1/160	0.016	0.013	0.018	0.075

very good agreement with the references solutions from de Vahl Davis [16] and Le Quéré [18]. The agreement is particularly good with the results of Le Quéré [18], who solved the problems by applying a pseudo-spectral method based on Chebyshev polynomials. The formulation was based on primitive variables, and the high accuracy of the solutions was ensured by increasing the spatial resolution up to a 128×128 polynomial expansion.

Figures 4–7 contain level curves for vorticity and temperature functions. An analysis of pictures shows that the flux is symmetric with respect to the centre for every Ra. At $Ra = 10^4$ the main feature of the flow is a central elliptic vortex, and the heat transfer is mainly due to conduction (vertical isotherms). For $Ra = 10^5$, the vortex breaks into two vortices moving toward the vertical walls, for higher values of Ra, a third, weaker vortex is observed. Increasing Ra causes a change of heat transfer mechanism. In fact, convection tends to become

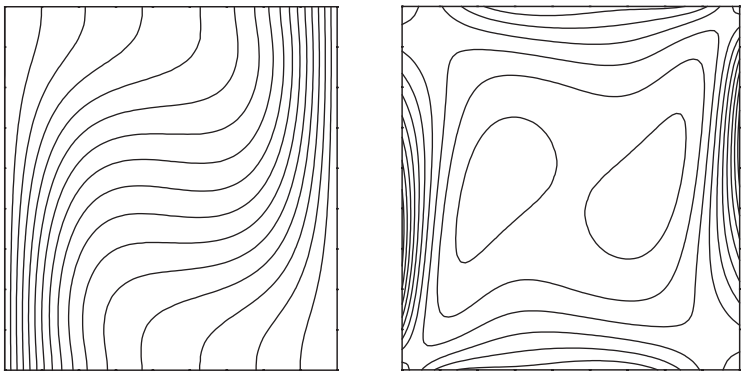

Figure 4. Isothermal lines (left) and isovorticity lines (right) at $Ra = 10^4$.

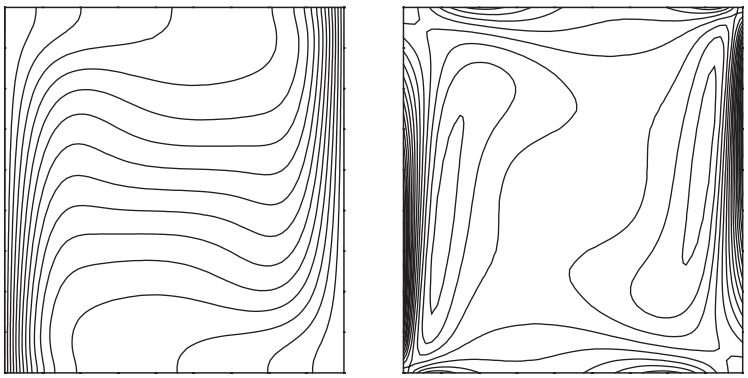

Figure 5. Isothermal lines (left) and isovorticity lines (right) at $Ra = 10^5$.

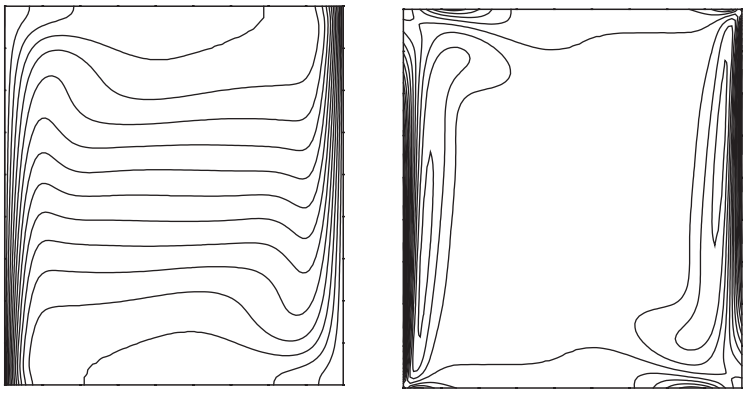

Figure 6. Isothermal lines (left) and isovorticity lines (right) at $Ra = 10^6$.

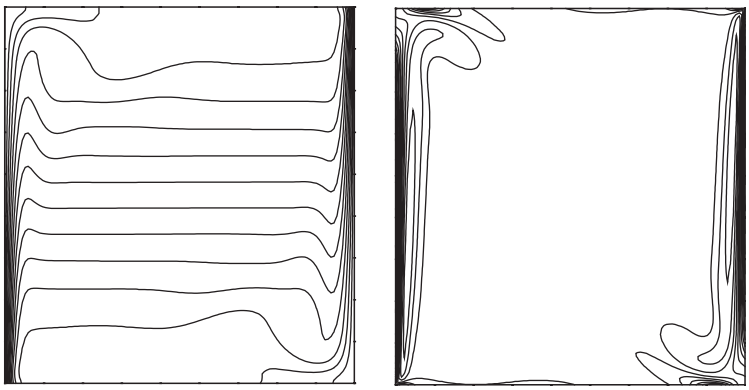

Figure 7. Isothermal lines (left) and isovorticity lines (right) at $Ra = 10^7$.

Table X. Comparison of results from the current compact fourth-order method and the stable fourth-order method in Choo and Schultz [9] for $Pr = 0.0001$ and $Ra = 100$.

Reference	n	$\lvert\psi_{\text{mid}}\rvert$	Nu
Present method	60	0.1007	1.0008
	80	0.0986	1.0008
Choo and Schultz [9]	80	0.1033	0.9995

Table XI. Comparison of results from the current compact fourth-order method and the stable fourth-order method in Choo and Schultz [9] for $Pr = 10$ and $Ra = 100$ as a function of n.

Methods		$n = 10$	$n = 20$	$n = 40$	$n = 60$	$n = 80$
Present compact	Nu	1.0022	1.0015	1.0014	1.0014	1.0014
fourth-order	$\lvert\psi_{\text{mid}}\rvert$	0.1257	0.1263	0.1264	0.1264	0.1264
scheme	$\lvert\zeta_{\text{mid}}\rvert$	3.5048	3.5184	3.5187	3.5176	3.5159
Stable	Nu	0.9903	0.9958	0.9982	0.9988	0.9980
fourth-order	$\lvert\psi_{\text{mid}}\rvert$	0.1248	0.1259	0.1262	0.1263	0.1263
method [9]	$\lvert\zeta_{\text{mid}}\rvert$	3.494	3.508	3.515	3.517	3.517

dominant: The isotherms are vertical everywhere, being horizontal only in the neighbourhood of vertical walls (very thin thermal boundary layer).

In addition, a collection of results from 37 sources is summarized in Reference 15. One source used a mesh size $n = 80$ for $Ra = 10^6$, but had difficulties preserving the symmetry of the problem. Also, none of the methods in References [4, 8, 15–19] indicates success with small Pr. But the present method produced results for a wide range of Pr. Table X compares the results of the present method with those of Choo and Schultz [9] for $Pr = 0.0001$ and $Ra = 100$, and Table XI shows the results for $Pr = 10$ and $Ra = 100$. Our numerical results showed that for $Pr > 1$ the present method converged very nicely. The results did not show any change for $Pr > 10$, $Ra = 100$.

5. CONCLUSION

In this work we have developed a new compact fourth-order scheme for the time-independent stream function–vorticity form of the two-dimensional, incompressible Navier–Stokes/Boussinesq equations governing the fluid flow and heat transfer. We have tested the present method for one problem, which has exact solutions and solved the heated cavity problem. The effectiveness of the developed method is exhibited from the numerical results. The key point with the present scheme is that it allows direct iteration for low-to-high *Ra*. It is the success of the current method with the wide range of *Ra*, *Pr* and mesh sizes that indicates the potential of this method as an accurate and stable numerical method applicable to a wide range of problems.

APPENDIX A

This appendix presents a brief derivation of the formula (70). Using Taylor series at an arbitrary node (x_0, y_j) along the vertical wall $x=0$, we have

$$T_{1,j}+\delta T_{2,j}=(1+\delta T_{0,j}+h(1+2\delta)(T_x)_{0,j}+(h^2/2)(1+4\delta)(T_{xx})_{0,j}+(h^3/6)(1+8\delta)(T_{xxx})_{0,j} +(h^4/24)(1+16\delta)(T_{xxxx})_{0,j}+O(h^5) \tag{A1}$$

Using (2), $(T_{xx})_{0,j}$ in (A1) can be written as

$$(T_{xx})_{0,j}=(-T_{yy}+\psi_y T_x-\psi_x T_y)_{0,j}=0 \tag{A2}$$

where we have used the fact that $(\psi_x)_{0,j}=0$, $(\psi_y)_{0,j}=0$ and $(T_{yy})_{0,j}=0$ on the vertical wall $x=0$. Furthermore, differentiating (A2),

$$(T_{xxx})_{0,j}=(-T_{yyx}+\psi_{xy}T_x+\psi_y T_{xx}-\psi_{xx}T_y-\psi_x T_{xy})_{0,j}=(-T_{yyx})_{0,j} \tag{A3}$$

where we have used the fact that $(\psi_x)_{0,j}=0$, $(\psi_y)_{0,j}=0$, $(\psi_{xy})_{0,j}=0$, and $(T_y)_{0,j}=0$ on the vertical wall $x=0$.

Substituting (A2) and (A3) into (A1), and setting $\delta=-\frac{1}{16}$, gives

$$16T_{1,j}-T_{2,j}=15T_{0,j}+14h(T_x)_{0,j}+(4h^3/3)(T_{yyx})_{0,j}+O(h^5) \tag{A4}$$

Thus, if we use

$$(T_{yyx})_{0,j}=[-3(T_{0,j+1}-2T_{0,j}+T_{0,j-1})+4(T_{1,j+1}-2T_{1,j}+T_{1,j-1}) -(T_{2,j+1}-2T_{2,j}+T_{0,j-1})]/(2h^3)+O(h^2) \tag{A5}$$

to substitute for $(T_{yyx})_{0,j}$, the resulting fourth-order formula is

$$(T_x)_{0,j}=(-15T_{0,j}+16T_{1,j}-T_{2,j})/(14h) +[-3(T_{0,j+1}-2T_{0,j}+T_{0,j-1})+4(T_{1,j+1}-2T_{1,j}+T_{1,j-1}) -(T_{2,j+1}-2T_{2,j}+T_{0,j-1}))/(21h)+O(h^4) \tag{A6}$$

ACKNOWLEDGEMENTS

This work is supported by the National Natural Science Foundation of China under Grant 19702008, TRAPOYT and the High Performance Computing Foundation of China under Grant 99107 and 00108.

REFERENCES

1. Morton KW. *Numerical Solution of Convection-Diffusion Problems*. Chapman & Hall: London, 1996.
2. Brandt A, Yavenh I. Inadequency of first-order upwind difference schemes for some recirculating flow. *Journal of Computational Physics* 1991; **93**:128–143.
3. Zhang J. Accelerated high-accuracy multigrid solution of the convection–diffusion equation with high Reynolds number. *Numerical Methods for Partial Differential Equations* 1997; **13**:77–92.
4. Dennis SCR, Hudson JD. Compact h^4 finite-difference approximations to operators of Navier–Stokes type. *Journal of Computational Physics* 1989; **85**:390–416.
5. Gupta MM. High accuracy solutions of incompressible Navier–Stokes equations. *Journal of Computational Physics* 1991; **93**:343–359.
6. Spotz WF, Carey GF. High-order compact scheme for the steady stream-function vorticity equations. *International Journal for Numerical Methods in Engineering* 1995; **38**:3497–3512.
7. Li M, Tang T, Fornberg B. A compact fourth-order finite difference scheme for the incompressible Navier–Stokes equations. *International Journal for Numerical Methods in Fluids* 1995; **20**:1137–1151.
8. Chen GQ, Gao Z, Yang ZF. A perturbational h^4 exponential finite difference scheme for convection diffusion equation. *Journal of Computational Physics* 1993; **104**:129–139.
9. Choo JY, Schultz DH. A stable high order method for the heated cavity problem. *International Journal for Numerical Methods in Fluids* 1992; **15**:1313–1332.
10. Tian ZF, Cui J. A new method of constructing fourth-order compact scheme for the steady convection–diffusion equation. In *Proceedings of The 7th International Symposium on Computational Fluid Dynamics*, Beijing, China, Zhuang FG (ed.), International Academic Publishers: Beijing, 1997; 116–121.
11. Gupta MM, Manohar RP, Stephenson JW. A single cell high order scheme for the convection–diffusion equation with variable coefficients. *International Journal for Numerical Methods in Fluids* 1984; **4**:641–651.
12. Tian ZF, Cui Y. Fourth-order compact finite-difference method for the steady three-dimensional convection-diffusion equation. In *Proceedings of The 6th EPMESC Conference*, Guangzhou, China, Han Dajian, Mo Haihong (ed.), South China University of Technology Press: Guangzhou, 1997; 286–491.
13. Hirsh RS. Higher order accurate difference solutions of fluid mechanics problems by a compact differencing technique. *Journal of Computational Physics* 1975; **19**:90–109.
14. Spotz WF. Accuracy and performance of numerical wall boundary conditions for steady, 2D, incompressible stream-function vorticity. *International Journal for Numerical Methods in Fluids* 1998; **28**:737–757.
15. De Vahl Davis G, Jones IP. Natural convection in a square cavity:a comparison exercise. *International Journal for Numerical Methods in Fluids* 1983; **3**:227–248.
16. De Vahl Davis G. Natural convection of air in a square cavity:a bench mark numerical solution. *International Journal for Numerical Methods in Fluids* 1983; **3**:249–264.
17. Hortmann M, Perić M. Finite volume multigrid prediction of laminar natural convection:bench-mark solutions. *International Journal for Numerical Methods in Fluids* 1990; **11**:189–207.
18. Le Quéré P. Accurate solution to the square thermally driven cavity at high Rayleigh number. *Computers and Fluids* 1991; **20**:29–41.
19. Syrjälä S. Higher order Penalty–Galerkin finite element approach to laminar natural convection in a square cavity. *Numerical Heat Transfer*, *Part A* 1996; **29**:197–210.
20. Gupta MM, Manohar RP. Boundary approximations and accuracy in viscous flow computations. *Journal of Computational Physics* 1978; **31**:265–288.

